J Eng Math (2009) 63:327–338
DOI 10.1007/s10665-007-9196-9

Higher-order asymptotics for edge-buckling of pre-stressed thin plates under in-plane bending

Ciprian D. Coman · Andrew P. Bassom

Received: 1 March 2007 / Accepted: 3 September 2007 / Published online: 27 September 2007

Abstract Singular perturbation techniques are used to investigate the linear eigenvalue problem that describes the partial wrinkling of a pre-stressed rectangular thin elastic plate under in-plane bending. The dependence of the critical load and the wavelength of the localised oscillatory pattern on the non-dimensional bending rigidity of the plate is captured with a higher-order boundary-layer analysis. Comparisons with direct numerical simulations of the original eigenproblem confirm the accuracy and versatility of the asymptotic technique explored in this work.

Keywords Boundary layers · Eigenvalue problems · Thin elastic plates · Wrinkling

1 Introduction

Within classical plate theory many problems involving the linear stability analysis of stretched thin elastic films under the action of in-plane forces can be cast as a singularly perturbed fourth-order partial differential equation for the out-of-plane displacement (see [1, Chap. 4], for example). More specifically, if $u \equiv u(\xi_1, \xi_2)$ represents this displacement function in some suitably chosen system of curvilinear coordinates (ξ_1, ξ_2), then it can be shown that it satisfies an equation of the form

$$\varepsilon \mathcal{M}[u] + \mathcal{N}[u; \lambda, \mathring{\boldsymbol{\sigma}}] = 0, \tag{1}$$

which must be supplemented with a suitable set of boundary conditions. Here, $\mathcal{M}$ and $\mathcal{N}$ are partial differential operators associated with the bending and the stretching contributions to the total energy of the plate, respectively, while λ denotes the loading parameter, and $\mathring{\boldsymbol{\sigma}} = (\mathring{\sigma}_{\xi_i \xi_j})_{i,j=1,2}$ is the tensor that characterises the pre-bifurcation state of plane stress due to applied forces. Furthermore, $0 < \varepsilon \ll 1$ is a characteristic length-scale dictated by both the geometry and the mechanics of the problem under investigation.

The existence of possible instabilities in such thin plates requires that at least one of the principal stresses of $\mathring{\boldsymbol{\sigma}}$, say σ_1 or σ_2, becomes negative (the direction of these principal stresses need not be the same as ξ_1 or ξ_2, cf. [2]). In that case the instability is characterised by a sinusoidal rippling pattern, and the questions of interest in

C. D. Coman (✉)
Department of Mathematics, University of Glasgow, University Gardens, Glasgow G12 8QW, Scotland, UK
e-mail: cdc@maths.gla.ac.uk

A. P. Bassom
School of Mathematics and Statistics, University of Western Australia, Crawley 6009, Australia

relation to Eq. 1 include finding the critical $\lambda \equiv \lambda_\varepsilon$ for which the instability is triggered, as well as the number of wrinkles associated with it, $m \equiv m_\varepsilon$. Owing to the presence of the small parameter ε, one is naturally led to consider the reduced problem obtained by setting $\varepsilon = 0$ in (1). However, the corresponding equation is that of a (inhomogeneously) pre-stressed membrane under the action of in-plane forces, and thus compressive stresses are prohibited. The usual point of view adopted in the literature is that, if one of the principal stresses becomes negative, the instability pattern displayed by the membrane contains an infinite number of wrinkles perpendicular to the direction(s) of compressive stresses; in other words, $m_0 = \infty$. Various tension-field theories are able to describe what happens after the onset of wrinkling by allowing for a variable Poisson ratio (for example, see [3–5]) or a relaxed strain-energy function [6,7]. However, within this framework only the extent of the wrinkled regions and the directions of wrinkles can be obtained and issues like the critical load and the preferred number of wrinkles remain unknown. Nevertheless, tension-field theories are very powerful methods which are designed for analysing post-buckling regimes; in contrast, our main interest resides with a buckling analysis.

Here, we shall not address the problem (1) in any generality. Rather we shall show, for a specific problem, how singular perturbation techniques can be applied to yield higher-order asymptotic approximations for the critical load and the corresponding number of wrinkles. The focus of our investigation is with the instability of a pre-stressed rectangular thin elastic plate under in-plane bending, a problem that was discussed in [8] using WKB theory. The associated linear eigenproblem was cast in the form (1), with only one of the principal stresses capable of taking negative values for sufficiently large loading, thus leading to a homogeneous rippling deformation. The determination of the critical load was based on a normal mode approach which essentially reduces (1) to an eigenvalue problem for an ordinary differential equation containing not only λ but also m. The dependence on this latter parameter is non-trivial as this quantity is unknown a priori, and finding those values of m that render the minimum of λ was not possible. Instead, the eigenvalue was determined as a function of both ε and the number of wrinkles. It was shown that the formulae obtained were very accurate but, unfortunately, the question still remains as to the critical wrinkling number in terms of the controlling parameters of the problem; the issue that is taken up here. As we shall see shortly, this requires a change of tack, as a classical boundary-layer analysis seems to be a more fruitful approach. We are motivated by recent work [9] in which we used boundary-layer arguments to reveal the preferred wrinkling mode of a radially stretched annular thin plate. Only a leading-order analysis was conducted in that investigation, and the boundary conditions involved were fairly simple. In contrast, in the next sections we shall allow more flexibility for the constraints imposed on the edges of the elastic plate, and the asymptotics are carried out to higher orders. The effect of accounting for various edge conditions is reflected in different structures of the boundary layers, which in turn has implications for the accuracy of the results obtained.

The problem under investigation in this study is a further example of the relevance of *nested boundary layers* in problems of elastic stability. Although these entities are common in fluid mechanics, they seem to have been largely overlooked in the solids literature. Reissner [10] appears to be the first to have realised that, for certain ranges of parameters, boundary layers at the edges of thin shells are such that within one boundary layer of specified width there is buried an asymptotically thinner second layer. The works of Ranjan and Steele [11], Taber [12], Movchan and Movchan [[13], pp. 238–246], and Fu [14] also contain interesting related phenomena, and include detailed information and pointers to the relevant literature.

Undoubtedly, the understanding of wrinkling instabilities exhibited by very thin elastic plates is an important topic as revealed by many recent investigations. We remark here that rectangular geometries seem to be prevalent (see [8,15–17]), but thin annular plates pose interesting challenges as well [2,9,18–20] and are relevant to important biomechanical applications (e.g., [21,22]).

To keep the paper reasonably self-contained, we start our study with a brief recap of the mathematical model introduced in [8]. In Sect. 3 the structure of the main boundary layer is unravelled, and the first correction terms in the asymptotic expansions of the quantities of interest are calculated. It turns out that further corrections require the consideration of a secondary (bending) boundary layer. Since we are interested in broadening the range of applicability of the theoretical device employed in [9], we treat two distinct types of boundary conditions. Section 4.1 deals with the situation when two edges of the film are clamped while in Sect. 4.2 we adapt that analysis for a pair of free edges. The validity of the asymptotic work is confirmed in Sect. 5 by comparisons with direct numerical

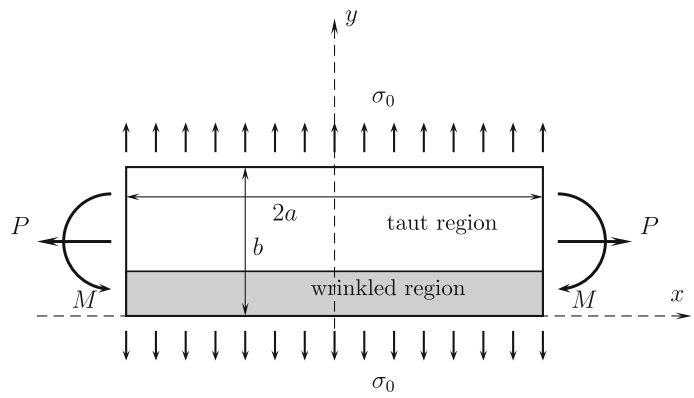

Fig. 1 Stretched thin plate under in-plane bending

simulations of the original eigenproblem. The paper concludes with a discussion of our main findings, together with suggestions for further study.

2 Outline of the problem

A full description of the model adopted in this work was given in [8], to which the reader is referred for more details. We consider a rectangular thin plate of length $2a$, width b, and thickness h ($h/b \ll 1$), corresponding to the situation illustrated in Fig. 1. We assume the plate to be initially stretched by imposing the normal stress σ_0 in the y-direction, on the edges $y = 0,\ b$, and an axial load $P = \sigma_0 hb$ in the x-direction, acting at the midpoints of the lateral sides. A bending moment, M, is assumed to act as indicated in Fig. 1, whose net effect is to introduce a destabilising feature into this configuration. The non-homogeneous pre-bifurcation state of stress is taken to be independent of the longitudinal coordinate x (cf. [3,23]), an assumption that allows us to express these stresses in a simplified analytical form. Finally, the bifurcation equation for the out-of-plane displacement, $w(x,\ y)$, is obtained from the classical plate theory (see [1], for example), and corresponds to a linearised version of the Donnell-von Kármán equations. After suitable non-dimensionalisation the resulting equation can be written

$$\varepsilon^2 \Delta^2 w - 6\left[2\lambda y - \left(\lambda - \frac{1}{6}\right)\right]\frac{\partial^2 w}{\partial x^2} - \frac{\partial^2 w}{\partial y^2} = 0 \quad \text{for } (x,\ y) \in (-\eta,\ \eta) \times (0,\ 1), \tag{2}$$

where

$$\eta := \frac{a}{b}, \quad \lambda := \frac{M}{Pb}, \quad \varepsilon^2 := \frac{1}{12(1-\nu^2)}\left(\frac{E}{\sigma_0}\right)\left(\frac{h}{b}\right)^2$$

and E and ν denote the Young's modulus and Poisson's ratio of the plate material. The rescaling employed above is valid only for $\sigma_0 \neq 0$ (and hence $P \neq 0$). This assumption is not restrictive because the singular case $\sigma_0 = 0$ corresponds to a situation in which there is no initial pre-stress present in the plate; the solution of the resulting stability problem is well known and can be found, for example, in the classical text by Timoshenko [24].

Assuming that the two lateral edges $x = \pm\eta$ are simply supported, we can simplify Eq. 2 further by adopting a normal-mode approach. On seeking solutions with

$$w(x,\ y) := W(y)\sin(A_m x), \tag{3}$$

where $A_m := m\pi/\eta$ and $m \in \mathbb{N}$ is the mode number (the number of identical sinusoidal half-waves parallel to the y-axis), the infinitesimal amplitude $W \equiv W(y)$ of these solutions satisfies the singularly perturbed differential equation

$$W'''' + \mathcal{P}(\mu,\ A_m)W'' + \mathcal{Q}(y;\ \mu,\ A_m)W = 0, \tag{4}$$

with

$$\mathcal{P}(\mu,\ A_m) := -(\mu^2 + 2A_m^2), \quad \mathcal{Q}(y;\ \mu,\ A_m) := A_m^2\left\{A_m^2 + 6\mu^2\left[2\lambda y - \left(\lambda - \frac{1}{6}\right)\right]\right\},$$

where $\mu := 1/\varepsilon$ is a large parameter. Here dashes indicate differentiation with respect to y, and occasionally higher-order derivatives will be denoted by superscripts enclosed between parentheses.

The original boundary conditions considered in [8] were based on the assumption that the edges $y = 0$ and $y = 1$ are free, so that $W(y)$ must be found subject to

$$W'' - \nu A_m^2 W = 0 \qquad \text{at } y = 0,\ 1, \tag{5a}$$

$$W''' - \left[\mu^2 + (2-\nu)A_m^2\right]W' = 0 \quad \text{at } y = 0,\ 1. \tag{5b}$$

In order to explore the significance of the boundary conditions on the asymptotic method investigated in this work, we shall also allow for the case when the two horizontal edges are clamped. The effect of this choice translates into the simpler constraints

$$W = W' = 0 \quad \text{at } y = 0, 1. \tag{6}$$

In [8] the first author used a WKB method to derive very accurate approximations for the eigenvalues of the problem (4)–(5), in the form

$$\lambda = \frac{1}{6}(\alpha^2+1) + \frac{|\,\zeta_0|}{3\sqrt[3]{2}}(\alpha^2+1)^{2/3}A_m^{-2/3} + \frac{2\sqrt[3]{2}}{9}\,|\,\zeta_0|^2(\alpha^2+1)^{1/3}A_m^{-4/3} + \frac{2}{9}\,|\,\zeta_0|^3A_m^{-2} + \mathcal{O}(A_m^{-8/3}), \tag{7}$$

where $\alpha := A_m/\mu \ll 1$ and ζ_0 is the first zero of the equation $\mathrm{Ai}'(\zeta) = 0$ (Ai is the usual Airy function of the first kind). This formula is valid provided that $1 \ll A_m \ll \mu$ but, for a given η, the size of the minimum eigenvalue is unclear as is the mode number for which that minimum is attained; all that is known is that the least eigenvalue will be found within the range $\mathcal{O}(\mu^{1/2}) \le A_m \ll \mu$. From a practical point of view these questions are probably more important than knowing λ expressed as a function of all the parameters that feature in the problem. It is this aspect of [8] which motivated the present investigation. The key observation for what follows is that the minimum λ corresponds to the presence of a turning point in the differential equation (4), which is asymptotically close to the edge $y = 0$. Furthermore, as $\mu \to \infty$ (i.e., the thin plate approximates an ideal membrane), the number of wrinkles grows with μ, so we can expand the eigenfunctions, eigenvalues and mode number in suitable (fractional) powers of $\mu \gg 1$. The implementation of this plan is carried out next.

3 The main-layer problem

A careful inspection of the WKB analysis explored in [8] suggests that, when $A_m = \mathcal{O}(\mu^{3/4})$, the turning-point problem resides in the region where $y = \mu^{-1/2}Y$, $Y = \mathcal{O}(1)$. Solutions are sought with

$$W(Y) = W_0(Y) + W_1(Y)\mu^{-1/2} + W_2(Y)\mu^{-1} + \cdots, \tag{8a}$$

$$\lambda = \lambda_0 + \lambda_1\mu^{-1/2} + \lambda_2\mu^{-1} + \lambda_3\mu^{-3/2} + \cdots, \tag{8b}$$

$$A_m^2 = M_0\mu^{3/2} + M_1\mu + M_2\mu^{1/2} + \ldots, \tag{8c}$$

where the functions $W_j(Y)$ and the coefficients λ_j, M_j $(j \ge 0)$ are to be found by substituting (8) in (4). At leading order this process results in an algebraic relation, which is then followed by a series of variable-coefficient differential equations:

$$\mathcal{O}(\mu^{7/2}) : 6M_0W_0\left(\lambda_0 - \frac{1}{6}\right) = 0, \tag{9a}$$

$$\mathcal{O}(\mu^3) : \mathcal{L}_M[W_0] = 0, \tag{9b}$$

$$\mathcal{O}(\mu^{3-j/2}) : \mathcal{L}_M[W_j] = \sum_{i=1}^{j} \mathcal{R}_i[W_{j-i}] - \frac{\mathrm{d}^4 W_{j-2}}{\mathrm{d}Y^4} \quad (j \geq 1), \tag{9c}$$

with the convention in (9c) that $W_{-1}(Y) \equiv 0$. The differential operators that appear in (9) are defined according to

$$\mathcal{L}_M := -\frac{\mathrm{d}^2}{\mathrm{d}Y^2} + M_0(M_0 - 6\lambda_1 + 2Y), \tag{10}$$

$$\mathcal{R}_i := 2M_{i-1}\frac{\mathrm{d}^2}{\mathrm{d}Y^2} - \left[\sum_{k=0}^{i} M_k M_{i-k} + 12Y\left(\sum_{k=0}^{i} M_k\lambda_{i-k}\right) - 6\left(\sum_{k=0}^{i} M_k\lambda_{i+1-k}\right)\right]. \tag{11}$$

The solution of (9a) is simply $\lambda_0 = 1/6$ and, as expected, this coincides with the wrinkling load for an ideal membrane ($\mu \to \infty$). Subsequent terms in the expansion of the eigenvalue (8b) capture the increase in the load-carrying capacity of the thin plate due to the presence of finite bending rigidity.

On defining

$$C := \frac{1}{2}M_0 - 3\lambda_1, \tag{12}$$

and introducing the change of variable $Z = (2M_0)^{1/3}(Y + C)$, it follows from (9b) that

$$W_0(Y) = \mathrm{Ai}(Z), \tag{13}$$

where the (arbitrary) constant of proportionality has been chosen conveniently to be unity. It is clear that the solution (13) cannot fulfil both boundary conditions described by either (5) or (6) at $Y = 0$. Thus we adopt the usual procedure of satisfying just one of these constraints, with the understanding that the correction needed to ensure the remaining condition will arise from a nested secondary layer (whose analysis will be undertaken in Sect. 4). When the edges $y = 0, 1$ are clamped, the constant C in (12) will be fixed by requiring that $W_0 = 0$ at $Y = 0$, whereas for the free-edge problem we demand $\mathrm{d}W_0/\mathrm{d}Y = 0$ at $Y = 0$. In either case,

$$\lambda_1 = \frac{1}{3}\left(\frac{\omega^3}{4} - \frac{\zeta_0}{\omega}\right), \tag{14}$$

where $\omega := (2M_0)^{1/3}$ but ζ_0 will have different interpretations according to the nature of the boundary conditions adopted. For the free-edge case, $\zeta_0 = \zeta_{01} \approx -1.01879$ is the first zero of the derivative of the Airy function, while for clamped edges $\zeta_0 = \zeta_{02} \approx -2.3381$ represents the first zero of the Airy function (for short, ζ_{0j} represents the first zero of $\mathrm{Ai}^{(j)}(\zeta) = 0$, $j = 1, 2$). Note that λ_1 is minimised when

$$M_0 = \begin{cases} M_{0C}^* \equiv \sqrt{2}\,(-\zeta_{02}/3)^{3/4} \approx 1.17306, & \text{for clamped edges,} \\ M_{0F}^* \equiv \sqrt{2}\,(-\zeta_{01}/3)^{3/4} \approx 0.62912, & \text{for free edges.} \end{cases} \tag{15}$$

Henceforth, the subscripts "C" and "F" are used for some of the values of M_j and λ_j in (8), to indicate their association with the clamped and, respectively, free-edge boundary-conditions calculations. In order to avoid overdoing the notation, we shall employ this convention on a limited basis.

Finding the other terms in the expansions recorded in (8) requires solving sequentially the Eqs. 9c. Routine manipulations show that a particular integral of the $\mathcal{O}(\mu^{5/2})$ equation is

$$W_1(Y) = \beta_1\mathrm{Ai}^{(1)}(Z) + \beta_2\mathrm{Ai}^{(3)}(Z), \tag{16}$$

where the superscripts on the Airy functions in the above expression denote differentiation with respect to Z, and

$$\beta_1 := \frac{1}{\omega^2}\left(2M_0M_1 - 6(M_0\lambda_2 + M_1\lambda_1) - 12C(M_0\lambda_1 + M_1\lambda_0)\right), \tag{17a}$$

$$\beta_2 := \frac{4}{\omega^3}\left(M_0\lambda_1 + M_1\lambda_0 - \frac{\omega^6}{12}\right). \tag{17b}$$

In a similar way we obtain

$$W_2(Y) = (\gamma_0 - \gamma_7)\mathrm{Ai}^{(1)}(Z) + \frac{\gamma_1}{2}\mathrm{Ai}^{(2)}(Z) + \frac{1}{3}(\gamma_2 + \gamma_6 - 3\gamma_8)\mathrm{Ai}^{(3)}(Z) + \frac{1}{4}(\gamma_3 + \gamma_7)\mathrm{Ai}^{(4)}(Z) + \frac{\gamma_4}{5}\mathrm{Ai}^{(5)}(Z) + \frac{1}{6}(\gamma_5 + \gamma_8)\mathrm{Ai}^{(6)}(Z), \tag{18}$$

where

$$\gamma_0 := \frac{1}{\omega^2}\left(M_1^2 + 2M_0M_2 - 6(M_0\lambda_3 + M_1\lambda_2 + M_2\lambda_1) - 12C(M_0\lambda_2 + M_1\lambda_1 + M_2\lambda_0)\right),$$

and

$$\gamma_1 := \beta_1^2, \quad \gamma_2 := -2M_1, \quad \gamma_3 := \beta_1\beta_2 - 2M_0\beta_1, \quad \gamma_4 := \omega^2,$$

$$\gamma_5 := -2M_0\beta_2, \quad \gamma_6 := \frac{12}{\omega^3}(M_0\lambda_2 + M_1\lambda_1 + M_2\lambda_0), \quad \gamma_7 := \frac{12\beta_1}{\omega^3}(M_0\lambda_1 + M_1\lambda_0), \quad \gamma_8 := \frac{\gamma_7\beta_2}{\beta_1}.$$

We note that the representations of W_j $(j = 0, 1, 2)$ found above apply equally well to both types of boundary conditions mentioned in Sect. 2. However, matching with the solutions in the secondary layer will involve the values of these functions and their derivatives at $Y = 0$, and that will lead to different results for the two cases.

4 The nested layer

Since the solution in the main layer falls short of satisfying one of the boundary conditions on $y = 0$, it is to be expected that there is a second inner zone in which the eigenfunction matches onto the $\mathcal{O}(\mu^{-1/2})$ solutions. A scaling analysis of (4) indicates the nested layer is of width $\mathcal{O}(\mu^{-1})$ and we consider the details of this region now.

To begin, we introduce the new variable $\overline{Y} = \mathcal{O}(1)$ such that $y = \mu^{-1}\overline{Y}$, and look for solutions of (4) with

$$\overline{W}(\overline{Y}) = \overline{W}_0(\overline{Y})\mu^{-1/2} + \overline{W}_1(\overline{Y})\mu^{-1} + \overline{W}_2(\overline{Y})\mu^{-3/2} + \cdots, \tag{19}$$

while λ and A_m^2 still expand as in (8b) and (8c). The usual substitutions lead to the four leading-order equations

$$\mathcal{L}_S[\overline{W}_0] = 0, \tag{20a}$$

$$\mathcal{L}_S[\overline{W}_1] = 2M_0\frac{\mathrm{d}^2\overline{W}_0}{\mathrm{d}\overline{Y}^2}, \tag{20b}$$

$$\mathcal{L}_S[\overline{W}_2] = 2M_0\frac{\mathrm{d}^2\overline{W}_1}{\mathrm{d}\overline{Y}^2} + 2M_1\frac{\mathrm{d}^2\overline{W}_0}{\mathrm{d}\overline{Y}^2} + \left(6M_0\lambda_1 - M_0^2\right)\overline{W}_0, \tag{20c}$$

$$\mathcal{L}_S[\overline{W}_3] = 2M_0\frac{\mathrm{d}^2\overline{W}_2}{\mathrm{d}\overline{Y}^2} + 2M_1\frac{\mathrm{d}^2\overline{W}_1}{\mathrm{d}\overline{Y}^2} + 2M_2\frac{\mathrm{d}^2\overline{W}_0}{\mathrm{d}\overline{Y}^2} + \left(6M_0\lambda_1 - M_0^2\right)\overline{W}_1 + \left[6(M_0\lambda_2 + M_1\lambda_1) - 2M_0M_1 - 2M_0\overline{Y}\right]\overline{W}_0, \tag{20d}$$

in which

$$\mathcal{L}_S := \frac{\mathrm{d}^4}{\mathrm{d}\overline{Y}^4} - \frac{\mathrm{d}^2}{\mathrm{d}\overline{Y}^2}.$$

The sequence of equations given in (20) must be supplemented with appropriate boundary conditions. It is at this stage that significant changes in the boundary-layer solutions for the two edge conditions start to surface and so, for the sake of clarity, we shall consider the two cases separately.

4.1 Clamped edges

Solving (20a) subject to $\overline{W}_0 = \mathrm{d}\overline{W}_0/\mathrm{d}\overline{Y} = 0$ at $\overline{Y} = 0$ gives

$$\overline{W}_0(\overline{Y}) = C_1(\exp(-\overline{Y}) + \overline{Y} - 1), \tag{21}$$

where $C_1 \in \mathbb{R}$ is found by matching with the $\mathcal{O}(\mu^{-1/2})$ term in the main layer; hence, $C_1 = \mathrm{Ai}'_0$, with $\mathrm{Ai}'_0 := \mathrm{Ai}'(\zeta_{02})$. Moreover, the constant term in (21) must also match on the form of $W_1(Y)$ as $Y \to 0$, and the resulting algebraic relation leads to

$$\lambda_{2C} = \frac{M_1}{6}\left(1 + \frac{4\zeta_{02}}{3\,\omega^4}\right) + \frac{1}{3}\left(1 - \frac{2}{3}\zeta_{02}\omega^2 + \frac{4\zeta_{02}^2}{3\,\omega^2}\right). \tag{22}$$

For $M_0 = M_{0C}^*$ the coefficient of M_1 in (22) vanishes. As we are about to see shortly, this feature is independent of the choice of boundary conditions and a similar phenomenon was encountered in the study of the annular plate discussed in [9] (although the eigenvalue problem investigated there was rather different). Recalling (9c) and the form of W_2 in (18), it follows that next-order matching gives λ_3 as a quadratic in M_1 and hence the critical value of $M_1 = M_{1C}^*$ can be readily identified.

To this end, the solution of (20b) can be cast in the form

$$\overline{W}_1(\overline{Y}) = C_2\exp(-\overline{Y}) + C_3\overline{Y} + C_4 - \frac{1}{2}M_0C_1(5 + 2\overline{Y})\exp(-\overline{Y}), \tag{23}$$

and satisfying the boundary conditions, $\overline{W}_1 = \mathrm{d}\overline{W}_1/\mathrm{d}\overline{Y} = 0$ at $\overline{Y} = 0$, gives two of the constants C_j $(j = 2, 3, 4)$ in terms of the third. Then, matching with the $\mathcal{O}(\mu^{-1})$ contribution in the main layer involves two conditions and permits the elimination of this third constant, leaving us with a relation that involves only the M_j's and λ_j's. The algebraic manipulations are routine but lengthy, so here we only state the outcome

$$15\,(2\gamma_0 + \gamma_3 - \gamma_7) + 10(\gamma_2 + \gamma_6 + 3\gamma_5)\zeta_{02} + 6\gamma_4\zeta_{02}^2 = 15\,\omega(\omega^3 - 4\beta_2). \tag{24}$$

Solving for λ_3 in (24) results in

$$\lambda_{3C} = 0.10643M_1^2 - 0.16974M_1 + 0.04123M_2 + 7.90251,$$

whose minimum is attained for

$$M_1 = M_{1C}^* \equiv 0.79737. \tag{25}$$

4.2 Free edges

In this case we need to amend the form of the ansatz (19) according to

$$\overline{W}(\overline{Y}) = \overline{W}_0(\overline{Y}) + \overline{W}_1(\overline{Y})\mu^{-1/2} + \overline{W}_2(\overline{Y})\mu^{-1} + \cdots, \tag{26}$$

where the unknown functions $\overline{W}_j(\overline{Y})$ $(j \geq 0)$ satisfy the same equations (20) recorded above. It is not immediately obvious that the matching procedure will succeed in fixing all the coefficients that appear in (8). For this reason we present this case in a little more detail.

As the solutions in the main layer are already available, we start by expressing $W(Y)$, as given by (8a), in terms of $\overline{Y}$. For $Y \to 0$ we find that

$$\begin{aligned} W = {} & \Gamma_{00} + \Gamma_{10}\mu^{-1/2} + \left(\frac{1}{2}\,\omega^2\Gamma_{02}\,\overline{Y}^2 + \omega\Gamma_{11}\,\overline{Y} + \Gamma_{20}\right)\mu^{-1} \\ & + \left(\frac{1}{6}\,\omega^3\Gamma_{03}\,\overline{Y}^3 + \frac{1}{2}\,\omega^2\Gamma_{12}\,\overline{Y}^2 + \omega\Gamma_{21}\,\overline{Y} + \Gamma_{30}\right)\mu^{-3/2} + \mathcal{O}(\mu^{-2}), \end{aligned} \tag{27}$$

with

$$\Gamma_{ij} := (\mathrm{d}^j W_i/\mathrm{d}Z^j)|_{Z=\zeta_{01}}, \quad \text{for } i \geq 0,\ j \geq 1,$$

and we shall define $\Gamma_{i0} \equiv W_i(\zeta_{01})$ for all $i \geq 0$.

At first order, we must solve (20a) subject to

$$\overline{W}_0'' = 0 \quad \text{and} \quad \overline{W}_0''' - \overline{W}_0' = 0 \quad \text{at } \overline{Y} = 0,$$

and then matching with the $\mathcal{O}(1)$ term in (27) yields $\overline{W}_0(\overline{Y}) \equiv \mathrm{Ai}_0$, where $\mathrm{Ai}_0 := \mathrm{Ai}(\zeta_{01})$.

The solution of the next-order equation (20b) has to match Γ_{10}; moreover, $\overline{W}_1$ must also satisfy the boundary conditions

$$\overline{W}_1'' = \nu M_0 \overline{W}_0 \quad \text{and} \quad \overline{W}_1''' - \overline{W}_1' = (2-\nu) M_0 \overline{W}_0' \quad \text{at } \overline{Y} = 0,$$

and so $\overline{W}_1(\overline{Y}) = \mathrm{Ai}_0(\beta_2 + \nu N_0 \exp(-\overline{Y}))$, with β_2 as defined in (17b).

The general solution of (20c) is

$$\overline{W}_2(\overline{Y}) = C_1 \exp(-\overline{Y}) + C_2 \overline{Y} + C_3 - \mathrm{Ai}_0 \left[\left(3M_0\lambda_1 - \frac{M_0^2}{2} \right) \overline{Y}^2 - \nu M_0^2 \left(\overline{Y} + \frac{5}{2} \right) \exp(-\overline{Y}) \right], \tag{28}$$

for some $C_j \in \mathbb{R}$ $(j = 1, 2, 3)$. (Notice that we are repeating the labels for arbitrary constants used in Sect. 4.1 to avoid a plethora of notation, but as the two calculations are entirely separate no confusion should arise.) Satisfying the boundary conditions

$$\overline{W}_2'' = \nu \left[M_0 \overline{W}_1 + M_1 \overline{W}_0 \right] \quad \text{and} \quad \overline{W}_2''' - \overline{W}_2' = (2-\nu) \left[M_0 \overline{W}_1' + M_1 \overline{W}_0' \right] \tag{29}$$

at $\overline{Y} = 0$ fixes the constants C_1 and C_2. The value of C_1 is immaterial at this stage but does play a role in obtaining $\overline{W}_3(\overline{Y})$, while the second condition in (29) gives $C_2 = -\mathrm{Ai}_0(\nu M_0)^2$. Enforcing the matching of the linear term in the $\mathcal{O}(\mu^{-1})$ part of (27) with its counterpart in $\overline{W}_2(\overline{Y})$ above permits us to pin down λ_2 in terms of M_1 and quantities already known, namely

$$\lambda_{2F} = \frac{M_1}{6} \left(1 + \frac{4\zeta_{01}}{3\,\omega^4} \right) + \frac{1}{3} \left(\frac{\nu^2 \omega^4}{4\zeta_{01}} - \frac{2}{3} \zeta_{01} \omega^2 + \frac{4\zeta_{01}^2}{3\,\omega^2} \right). \tag{30}$$

It should be noted that, just as in the analysis for the clamped edges, if $M_0 = M_{0F}^*$ the coefficient of M_1 in (30) vanishes. Hence we need to explore the matching relations at $\mathcal{O}(\mu^{-3/2})$. Another important observation at this juncture is that the quadratic terms in (27) and (28) are identical, a fact that confirms the consistency of our asymptotic expansions; we shall see shortly that this property is not a coincidence, and keeps recurring at higher orders too. Also, matching the free terms demands that $C_3 = \Gamma_{20}$ but this information will not be needed to the orders we require. Beyond this point the algebra becomes rather tedious and the symbolic manipulation package MAPLE was used for the remainder of this section. Only an outline of the calculations will be included here.

It is fairly easy to show that the differential equation (20c) admits a general solution of the form

$$\overline{W}_3(\overline{Y}) = C_7 \exp(-\overline{Y}) + C_8 \overline{Y} + C_9 + \Delta_1 \overline{Y}^3 + \Delta_2 \overline{Y}^2 + \Delta_3 \overline{Y} + \Delta_4, \tag{31}$$

where the expressions Δ_i $(i = 1, \ldots, 4)$ involve exponentials like $\exp(-\overline{Y})$, as well as M_j $(j = 0, 1)$ and λ_j $(j = 0, 1, 2)$. The values of C_7 and C_8 are obtained by using the corresponding boundary conditions

$$\overline{W}_3'' = \nu \left[M_0 \overline{W}_2 + M_1 \overline{W}_1 + M_2 \overline{W}_0 \right], \tag{32}$$

$$\overline{W}_3''' - \overline{W}_3' = (2-\nu) \left[M_0 \overline{W}_2' + M_1 \overline{W}_1' + M_2 \overline{W}_0' \right], \tag{33}$$

at $\overline{Y} = 0$. Since only the latter constant will enter into the matching process, we note that

$$C_8 = -\frac{1}{3} \nu M_0 \mathrm{Ai}_0 \left[M_0^2 \left(6\nu^2 - 11\nu - 6 \right) + 6\nu \left(M_0\lambda_1 + M_1\lambda_0 \right) + 36 \left(M_0\lambda_1 + \nu M_1 \lambda_0 \right) \right]$$

but do not record C_7. As $\overline{Y} \to \infty$ so $\overline{W}_3(\overline{Y})$ asymptotes to

$$\overline{W}_3 \to \Theta_3 \overline{Y}^3 + \Theta_2 \overline{Y}^2 + \Theta_1 \overline{Y} + \Theta_0, \tag{34}$$

where

$$\Theta_0 := C_9 + \mathrm{Ai}_0 \left[2M_0 M_1 - 6(M_0\lambda_2 + M_1\lambda_1) + 2M_0^2(M_0 - 6\lambda_1)\left(\frac{M_0\lambda_1 + M_1\lambda_0}{M_0^2} - \frac{4}{3} \right) \right],$$

$$\Theta_2 := \mathrm{Ai}_0 \left[M_0 M_1 + 4M_0^2 \left(2\lambda_1 - \frac{M_0}{3} \right) + (M_0\lambda_1 + M_1\lambda_0)(M_0 - 6\lambda_1) - 3(M_0\lambda_2 + M_1\lambda_1) \right],$$

$$\Theta_3 := \frac{1}{3} M_0 \mathrm{Ai}_0, \quad \Theta_1 := C_8 + 2M_0 \mathrm{Ai}_0.$$

The form (34) must match onto the $\mathcal{O}(\mu^{-3/2})$ contribution in the inner expansion of the outer layer, (27). It turns out that the equalities between the cubic and quadratic terms in the two expressions are identically satisfied, while the matching of the linear parts gives

$$3(5\gamma_1 + 8\gamma_4) + 30(\gamma_0 + \gamma_3)\zeta_{01} + 5(2\gamma_2 + 9\gamma_5 + 2\gamma_6 + 3\gamma_8)\zeta_{01}^2 + 6\gamma_4\zeta_{01}^3 = \frac{C_8}{\omega A i_0} + \omega^2. \tag{35}$$

Finally, this relation allows us to find λ_3 as a quadratic in M_1, whence the critical value of $M_1 = M_{1F}^*$ is easily found to be

$$M_{1F}^* \equiv 0.39579 + 0.66666\,\nu^2. \tag{36}$$

5 Validation of the asymptotics

The asymptotic expansion of the critical wrinkling load assumes the form

$$\lambda^* = \begin{cases} \lambda_0 + \lambda_{1C}^* \mu^{-1/2} + \lambda_{2C}^* \mu^{-1} + \mathcal{O}(\mu^{-3/2}), & \text{for clamped edges,} \\ \lambda_0 + \lambda_{1F}^* \mu^{-1/2} + \lambda_{2F}^* \mu^{-1} + \mathcal{O}(\mu^{-3/2}), & \text{for free edges,} \end{cases} \tag{37}$$

where $\lambda_0 = 1/6$; the other coefficients are defined by

$$\lambda_{ij}^* := \lambda_{ij}|_{M_0 = M_{0j}^*}, \quad \text{for} \quad i \in \{1, 2\}, \ \ j \in \{C, F\},$$

and are routinely calculated with the help of the previous formulae (14), (15), (22), (30). For the sake of completeness, we note that

$$\lambda_{1C}^* = 0.78204, \quad \lambda_{2C}^* = 2.62679,$$
$$\lambda_{1F}^* = 0.41941, \quad \lambda_{2F}^* = 0.65966 - 0.11111\,\nu^2.$$

According to (8c) and the definition of A_m (see Sect. 2), the critical mode number in the two cases can be written as

$$m_{cr} = \frac{\eta}{\pi} \left[\sqrt{M_{0j}^*}\, \mu^{3/4} - \frac{M_{1j}^*}{2\sqrt{M_{0j}^*}}\, \mu^{1/4} + \mathcal{O}(\mu^{-1/4}) \right], \quad j \in \{C, F\}, \tag{38}$$

where M_{0j}^*, M_{1j}^* ($j \in \{C, F\}$) are given by (15), (25), and (36); it is found that

$$\frac{m_{cr}}{\eta} = \begin{cases} 0.34475\mu^{3/4} - 0.11717\mu^{1/4} + \mathcal{O}(\mu^{-1/4}), & \text{for clamped edges,} \\ 0.25247\mu^{3/4} - (0.07941 + 0.13376\nu^2)\mu^{1/4} + \mathcal{O}(\mu^{-1/4}), & \text{for free edges.} \end{cases}$$

With these results to hand, our immediate objective is to assess their accuracy by comparisons with direct numerical simulations of the full eigenvalue problems given in Sect. 2. On fixing μ and the Poisson's ratio ν, the neutral

stability curves $\lambda = \lambda(\eta, m)$ can be easily calculated for each integer $m \geq 1$ by numerically integrating Eq. 4 with the boundary conditions (5) or (6). It is found convenient to cast the differential equation as

$$\frac{\mathrm{d}\mathbf{w}}{\mathrm{d}y} = \mathbf{A}(y;\ \lambda,\ m,\ \eta)\mathbf{w}, \quad 0 < y < 1 \tag{39}$$

by introducing the usual dependent variables,

$$w_1(y) := W(y), \quad w_2(y) := W'(y), \quad w_3(y) := W''(y), \quad w_4(y) := W'''(y), \tag{40}$$

and then letting $\mathbf{w} := [w_1,\ w_2,\ w_3,\ w_4]^T$. The expression of the matrix $\mathbf{A} \in M_{4\times 4}(\mathbb{R})$ can easily be found by carrying out the above substitutions, and the boundary conditions admit a similar representation in terms of w_j $(j = 1, \ldots, 4)$.

Since the first positive eigenvalue of (39) depends on the mode number (which is unknown at this stage), for all practical purposes it is the envelope of these curves that is of relevance. One way of obtaining this curve numerically (together with the corresponding critical values of $m = m_{cr}$) is to plot the curves λ vs. η for each $m = 1, 2, \ldots$ and then identify the minimum of each curve. This is a rather awkward technique, especially if one is interested in the dependence of m_{cr} on the large parameter μ. A much simpler procedure which is based on the numerical continuation software [25], and which works in a number of related situations, is described below.

By letting

$$V(y) := \frac{\partial W(y)}{\partial m},$$

and differentiating (4) with respect to the mode number, it is found that

$$V'''' + \mathcal{P}(\mu, A_m)V'' + \mathcal{Q}(y; \mu, A_m)V = -\frac{\partial \mathcal{P}}{\partial m}W'' - \frac{\partial \mathcal{Q}}{\partial m}W. \tag{41}$$

According to the well-known Fredholm condition, this inhomogeneous differential equation is solvable if and only if its right-hand side is orthogonal on the solutions of the homogeneous adjoint equation. Conveniently, the differential operator in (4) and the boundary conditions (5) or (6) are such that the corresponding problems are self-adjoint. In consequence, assuming further that $\mathrm{d}\lambda/\mathrm{d}m = 0$ (the criticality condition for λ and m), the solvability condition for (41) becomes

$$\int_0^1 \left\{ w_1 w_3 - \left[A_m^2 + 3\mu^2 \left(2\lambda y - \left(\lambda - \frac{1}{6} \right) \right) \right] w_1^2 \right\} \mathrm{d}y = 0. \tag{42}$$

By integrating (39) subject to the integral constraint (42) and the corresponding set of boundary conditions, one can track any of the parameters μ, λ, or m in terms of the remaining two. The important point to recognise here is that the last two parameters will be precisely those associated with the envelope of the neutral stability curves. The illustration of this strategy follows next.

First, we notice that for the clamped film there is no dependence on ν in either λ^* (37) or m_{cr} (38) but these quantities do exhibit a weak dependence on the Poisson's ratio in the case of free edges; see (30) and (36). For the sake of brevity, we shall take $\nu = 0.3$ and all the results presented are calculated for this particular value.

The first set of direct numerical simulations is showed in Fig. 2, where the asymptotic approximations given by the expansion of λ^* above are included as well. A detailed discussion of the neutral stability curves was provided in [8], so here we shall confine our attention only to aspects relevant to the current work. The values of the mode number m for the plots included in Fig. 2 correspond to the regime $\mathcal{O}(\mu^{1/2}) \leq A_m \ll \mu$. It is clear that the corrections provided by the term $\lambda_{2j}^*(j \in \{C, F\})$ in formula (37) suffice for a good agreement between the two sets of data but it is also apparent that the convergence in Fig. 2(*b*) is slower. Such an occurrence is not accidental, and a quick inspection of Sects. 4.1 and 4.2 suggests that this is to be expected as the structures of the secondary boundary layer in the two cases discussed are slightly different. The dependence of the critical mode number on μ is shown in Fig. 3, which provides further evidence as to the versatility of the asymptotic analysis explored in this paper. Both the one- and the two-term approximations supplied by (38) correlate very well with the numerical solution, and it seems that the increase of accuracy by including the term $M_{1j}^*(j \in \{C, F\})$ in that formula is modest.

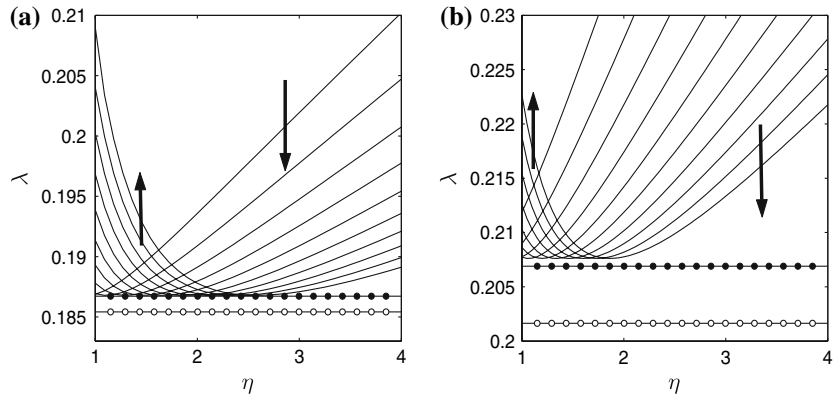

Fig. 2 Comparisons between the asymptotic approximations of the neutral stability curves and the direct numerical simulations of (4) for $\mu = 500$ and $\nu = 0.3$: (*a*) free-edge, and (*b*) clamped boundary conditions. The values of the mode number are $m = 5k$ for $5 \leq k \leq 14$, and the arrows indicate the direction of increasing m. In both windows the data points shown by black bullets represent the three-term asymptotic approximation derived from (37) while the open circles denote the two-term equivalent

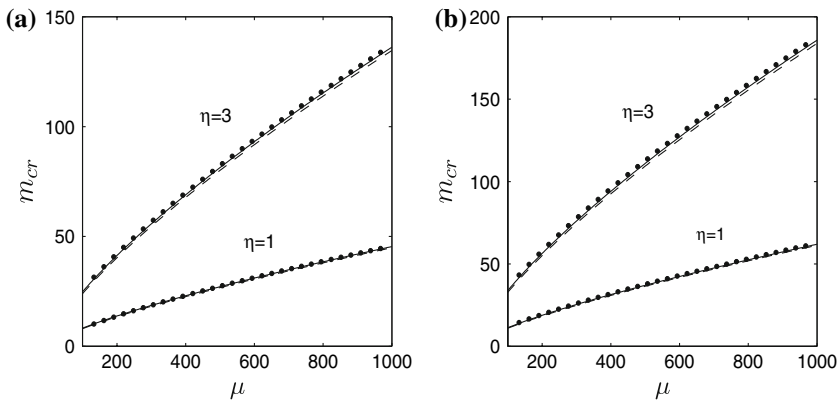

Fig. 3 Dependence of the critical mode number $m \equiv m_{cr}$ on the parameter $\mu \gg 1$. Both windows show results corresponding to $\eta = 1, 3$ for $\nu = 0.3$; (*a*) the free-edge case, (*b*) clamped boundary conditions. The black markers are obtained by numerically integrating (39) with the integral constraint (42); the continuous and dashed lines are the one- and, respectively, two-term asymptotic expressions obtained from (38)

6 Discussion

We have presented a complementary route to the WKB-type approach proposed in [8] for the localised wrinkling of a rectangular stretched thin plate under in-plane bending. A boundary-layer analysis has been carried out in order to capture the expressions of the critical wrinkling load as well as the wavelength of the instability pattern. The main advantage of this approach over the earlier analysis is that systematic higher-order calculations are possible with relative ease. Moreover, the numerical comparisons in Sect. 5 seem to indicate that accurate results are possible even with just a few terms in the corresponding asymptotic expansions. This aspect of the solution is corroborated by the results obtained recently in [9] for the related scenario of an annular thin film subjected to tensile loads along its edges.

The type of pre-stress adopted in this work amounts to all-round stretching, but the key ingredient in the analysis is the co-existence of compressive and tensile pre-buckling stresses. It is this particular feature that is responsible for the mixed elliptic/hyperbolic character of the bifurcation equation (2) and which leads to the localisation of the instability pattern. This is clearly not an isolated occurence. One can easily envisage other types of loadings or geometries where a similar analysis would apply, but finding a closed-form simple expression for the pre-buckling stress field is not always guaranteed. Such a difficulty arises, particularly, in [15] where a rectangular thin elastic

plate is subjected to opposite tensile forces on the short edges. Although the presence of compressive stresses in that context was checked numerically in the reference mentioned, an analytical expression is not available. In principle, finding the pre-buckling stress distribution in a particular problem would involve making some approximations like, for instance, adopting an axisymmetry assumption and/or relaxing the boundary conditions (i.e., working with generalised such conditions rather than their pointwise counterparts).

There are a range of extensions to the current work that can be considered. The azimuthal shearing of a stretched annular film [2] exhibits an instability akin to the one discussed in this paper, and is amenable to a similar method of solution. The main complication arising in such a context is that the eigenproblem is now governed by a set of two coupled fourth-order differential equations with (high-order) polynomial coefficients so that the approach employed here will require non-trivial modifications. Further research is suggested by the scaling of m_{cr} with μ. In the present investigation, as well as in [2,9], this scaling was found to obey a law of the form $m_{cr} \sim \mu^{3/4}$. This is a consequence of adopting the linearised Donnell–von Kármán buckling equation as the starting point for all three investigations but it is not clear whether the same qualitative behaviour will persists once the buckling equation is changed. Finally, it might be informative to examine the situation described in this paper within a nonlinear framework in order to gain an understanding of the limitations of the present analysis. All these aspects are currently being pursued and the results will be reported in due course.

Acknowledgements CDC acknowledges with gratitude the financial support received from The Royal Society for a visit to the University of Western Australia. We would like to thank the referees for their suggestions that have helped to improve the presentation of this work.

References

1. Alfutov NA (2000) Stability of elastic structures. Springer-Verlag, Berlin
2. Coman CD, Bassom AP (2007) Wrinkling of pre-stressed annular thin films under azimuthal shearing. Math Mech Solids (in press)
3. Stein M, Hedgepeth JM (1961) Analysis of partly wrinkled membranes. Technical Note, NASA-TN D-813
4. Mikulas MM (1964) Behaviour of a flat stretched membrane wrinkled by the rotation of an attached hub. Technical report, NASA-TN D-2456
5. Miller RK, Hedgepeth JM, Weingarten VI, Das P, Kahyai S (1985) Finite element analysis of partly wrinkled membranes. Comput Struct 20:631–639
6. Pipkin AC (1986) The relaxed energy density for isotropic elastic membranes. IMA J Appl Math 36:85–89
7. Steigmann D (1990) Tension field theory. Proc Roy Soc Lond A 429:141–173
8. Coman CD (2007) Edge-buckling in stretched thin films under in-plane bending. Z angew Math Phys 58:510–525
9. Coman CD, Bassom AP (2007) On the wrinkling of a pre-stressed annular film in tension. J Mech Phys Solids 55:1601–1617
10. Reissner E (1959) The edge effect in symmetric bending of shallow shells of revolutions. Commun Pure Appl Math 7:385–398
11. Ranjan GV, Steele CR (1980) Nonlinear correction for edge bending of shells. ASME J Appl Mech 47:861–865
12. Taber LA (1985) Nonlinear asymptotic solution of Reissner plate equations. ASME J Appl Mech 52:907–912
13. Movchan AB, Movchan NV (1995) Mathematical modelling of solids with non-regular boundaries. CRC Press, Boca Raton
14. Fu YB (1998) Some asymptotic results concerning the buckling of a spherical shell of arbitrary thickness. Int J Non-Lin Mech 33:1111–1122
15. Friedl N, Rammerstorfer FG, Fischer FD (2000) Buckling of stretched strips. Comput Struct 78:185–190
16. Cerda E, Mahadevan L (2003) Geometry and physics of wrinkling. Phys Rev Lett 90(7):1–4
17. Jacques N, Potier-Ferry M (2005) On mode localisation in tensile plate buckling. C R Mecanique 333:804–809
18. Géminard JC, Bernal R, Melo F (2004) Wrinkle formations in axisymmetrically stretched membranes. Eur Phys J E 15:117–126
19. Mora T, Boudaoud A (2006) Buckling of swelling gels. Eur Phys J E 20:119–124
20. Coman CD, Haughton DM (2006) Localised wrinkling instabilities in radially stretched annular thin films. Acta Mech 185:179–200
21. Harris AK, Wild P, Stopak D (1980) Silicone rubber substrata: a new wrinkle in cell locomotion. Science 208:177–179
22. Burton K, Taylor DL (1997) Traction forces of cytokinesis measured using optically modified elastic substrata. Nature 385:450–454
23. Månsson J, Söderqvist J (2003) Finite element analysis of thin membrane wrinkling. M.Sc. Thesis, Royal Institute of Technology (Stockholm)
24. Timoshenko SP (1961) Theory of elastic stability. McGraw-Hill, New York
25. Doedel EJ, Champneys AR, Fairgrieve TF, Kuznetsov YA, Sandstede B, Wang Y (1997) AUTO97: continuation and bifurcation software for ordinary differential equations. Technical report, Dept. of Computer Science, Concordia University, Montreal, Canada. Available by ftp from ftp.cs.concordia.caint/pub/doedel/auto